Optical transitions in dilute GaNAs nitrides: A comparison between and empirical pseudopotentials

G. Stenuit, S. Fahy

Author's Accepted Manuscript

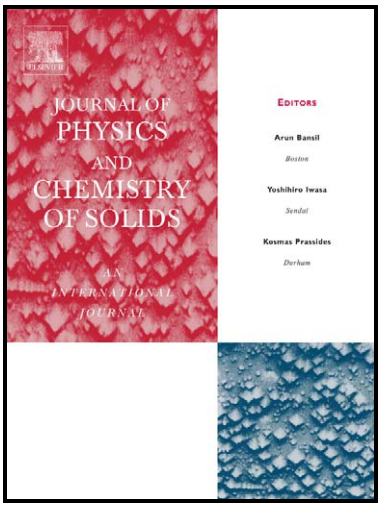

www.elsevier.com/locate/jpcs

Optical transitions in dilute GaN_xAs_{1-x} nitrides: A comparison between *ab initio* and empirical pseudopotentials

G. Stenuit, S. Fahy

PII: S0022-3697(09)00049-3
DOI: doi:10.1016/j.jpcs.2009.03.011
Reference: PCS 5810

To appear in: *Journal of Physics and Chemistry of Solids*

Received date: 26 November 2008
Revised date: 3 February 2009
Accepted date: 25 March 2009

Cite this article as: G. Stenuit and S. Fahy, Optical transitions in dilute GaN_xAs_{1-x} nitrides: A comparison between *ab initio* and empirical pseudopotentials, *Journal of Physics and Chemistry of Solids* (2009), doi:10.1016/j.jpcs.2009.03.011

Optical transitions in dilute GaN_xAs_{1-x} nitrides: A comparison between *ab initio* and empirical pseudopotentials

G. Stenuit[a,b,*], S. Fahy[a]

[a] *Tyndall National Institute, University College, Lee Maltings, Prospect Row, Cork, Ireland*
[b] *CNR-INFM DEMOCRITOS National Simulation Center, Theory@Elettra group, Area Science Park, Basovizza S.S. 14 Km 163.5, I-34012 Trieste, Italy*

Abstract

Ab initio Troullier-Martins and empirically adjusted Hartwigsen-Goedecker-Hutter pseudopotentials have been used, within the density functional theory (DFT) framework, to study the optical transitions in the dilute nitride, GaN_xAs_{1-x}. Composition dependence of the energy gap (E_-) and the E_+ optical transitions have been computed with the two pseudopotentials. Band anticrossing (BAC) model parameters have been derived from the composition dependence of the DFT E_- and E_+ optical transitions, providing DFT-based analytical expressions for $E_+(x)$ and $E_-(x)$. The influence of the N configuration (ordered or randomly distributed in the GaAs host material) has been studied. Random distribution is found to increase the energy gap E_-, compared to ordered structures, but has relatively little effect on the E_+ energy. Comparisons with the experimental and tight-binding data are reported.

Key words: semiconductors, ab initio calculations, optical properties
PACS: 71.55.Eq, 71.20.-b, 71.15.Mb

1. Introduction

The electronegativity and size difference between N and As anions induces many unusual features in the "highly mismatched" $GaAs_{1-x}N_x$ alloys. Besides the large reduction of the energy gap ($\sim 100-200$ meV for $\sim 1\%$ added in GaAs [1, 2, 3, 4]) and its composition-dependent bowing parameter [1], experimental [2, 3, 4] or theoretical [5] studies of N incorporation in GaAs also reveal a decrease of the lattice [6] and elastic [7, 8] constants, and a marked increase of the conduction effective mass [9, 10]. Other features, such as the presence of a highly localized vibrational mode around the N atom, have been observed experimentally and explained successfully within the first-principles framework [11, 12]. Dilute nitrides also exhibit a nitrogen-induced state (E_+) above the conduction band minimum, which has been observed in electroreflectance (ER) [13], photomodulated reflectance (PR) [14, 15] and high-pressure measurements [16]. In contrast to the redshift of the energy gap (E_-) with increasing nitrogen concentration, E_+ exhibits a blueshift whose rate is close to two-thirds of that of the E_- redshift.

In this paper, we focus on the optical properties in $GaAs_{1-x}N_x$ alloys, particularly on the composition dependence of the energy gap, its first derivative (dE_-/dx) and the E_+ energy level. The theoretical investigation of the composition dependence of the energy gap and its first derivative is motivated by their influence on the transport properties. In the S-matrix formalism [17], Fahy and O'Reilly [18] showed that, in the absence of N-N interactions, the n-type scattering cross section σ is proportional to the square of the derivative, $(dE_-/dx)^2$, of the energy gap E_- with respect to the N composition x, if the composition

*Corresponding author
Email addresses: stenuit@sissa.it (G. Stenuit)

dependence of the top of valence band E_v is neglected [1]. This formalism has successfully reproduced the experimental n- and p-type mobilities in the weakly scattering SiGe alloys from first-principles calculations [19, 20]. However, further calculations indicate that the mobility of carriers in dilute nitrides is substantially affected by N-N interactions [21].

Optical transition energies, in particular the band-gap, are often poorly reproduced by the DFT single-particle energy eigenvalues. In this paper, we examine an alternative approach, which returns partially to the original, empirical pseudopotential method [22]. We retain the self-consistency of the DFT mean-field approach, but empirically add extra terms to the atomic pseudopotentials in order to reproduce key features of the low-lying conduction band structures of GaAs and GaN. Our approach is therefore closely related to the "Darwin shift" used by Christensen [23] in the context of LMTO (linearized muffin-tin orbital) or the repulsive potential approach derived by Segev *et. al.* [24] in the context of LDA norm-conserving pseudopotential generation. Nevertheless, by opposition to the work done by Segev *et. al.* [24] where they apply a repulsive potential at the all electron stage of the pseudopotential generation, we have decided here to keep the initial *ab initio* PP and to tune directly only the local part to some selected electronic properties (see next section for further details). In addition, compared to works done by Christensen [23] in the context of LMTO (linearized muffin-tin orbital), we have used our empirical atomic potentials within the plane-wave LDA-DFT framework. Since the DFT band-gap problem is particularly severe in GaAs and GaN, and since the transport properties are closely related to the composition-dependence of the band-gap, the use of an empirical pseudopotential method may provide a better indication of material factors affecting the carrier mobility.

In the present work, we will use *Ab initio* Troullier-Martins [25] pseudopotentials and empirically adjusted Hartwigsen-Goedecker-Hutter (HGH) pseudopotentials [26] and a DFT treatment of the self-consistent electronic interactions [2] to find the optical transition energies. Analytical expressions for the composition dependence of E_- and E_+ are derived from the LDA-DFT electronic properties in supercells up to 512 atoms. The paper is organized as follows: The HGH pseudopotentials and our empirical approach are discussed in the Section II. Section III reports the optical transition energies for different N composition in dilute $GaAs_{1-x}N_x$ alloys, calculated using ordered DFT supercells; comparisons between the *ab initio* and empirical pseudopotentials, as well as with the experimental optical data, are given. Section IV studies the influence of random nitrogen distribution on the optical properties. Section V reports the overall conclusions and an appendix provides the parameters for the valence force field (VFF) method (derived from DFT calculations in medium-sized supercells), which is used in the structural optimization of large supercells.

2. Method of calculation

Ab initio methods based on density-functional theory (DFT) [27, 28] are by now common and well established tools for studying the structural properties of materials [29]. The plane-wave pseudopotential (PP) approach, combined to the local-density approximation (LDA), has provided a simple framework whose accuracy and predictive power for structural properties has already been demonstrated in a large variety of systems. Therefore, we use this LDA-DFT approach in finite "supercells" to represent the crystal. Because of the computational demands of structural optimization of systems with many atoms, the empirical valence force field (VFF) [30] method has also been to compute the atomic positions in supercells larger than 216 atoms. As described in detail in the Appendix, we derive the parameters of the VFF model from DFT calculations of GaAs, GaN and a supercell of $Ga_{32}As_{31}N$.

We have performed plane-wave pseudopotential LDA-DFT calculations with the `Abinit` package [31]. Lattice constants and atomic positions are found by total energy minimization in primitive 2-atom, bcc 32-atom, sc 64-atom and fcc 128-atom supercells. Equilibrium structures are achieved when the calculated

[1] Typically, $dE_v/dx << dE_c/dx$ in the dilute limit $x \to 0$

[2] Previous works done by Bellaiche *et al.* [5] did not include explicitly the LDA approximation for the exchange-correlation functional.

force on each atom is less than 5×10^{-5} Ha/Bohr. In larger supercells (sc 216-atom, bcc 256-atom and sc 512-atom), the VFF method has been used to compute the equilibrium position of the atoms (see Appendix for further details). The lattice constant has been assumed to follow the linear Vegard's law (in agreement with our previous LDA-DFT calculations [8]) for its composition dependence. In the ordered supercells (see Section III), one arsenic atom has been replaced by a nitrogen atom and the high point-group symmetry (O_h with 48 symmetry operations) gives a greatly reduced computational time.

Brillouin Zone integrations are performed with converged uniform $4 \times 4 \times 4$ $\vec{k}$-point meshes for the sc 8-atom, fcc 16-atom and bcc 32-atom supercells, $2 \times 2 \times 2$ $\vec{k}$-point meshes for the sc 64-atom and fcc 128-atom supercells [3] and $1 \times 1 \times 1$ $\vec{k}$-point meshes in the sc 216-atom, bcc 256-atom and sc 512-atom supercells. Convergence of the ground state energy is achieved with a plane-wave cutoff energy of 25 Ha.

For the DFT band structure calculations, the pseudopotentials (PP) used are of the Troullier-Martins type [25] provided by `abinit`. The LDA-DFT energy gaps computed from Troullier-Martins pseudopotentials (3d state excluded) are 0.515 eV and 2.113 eV for the bulk GaAs and GaN, respectively, which greatly underestimate [32, 33, 34] the experimental band gaps $E_g^{GaAs} = 1.52$ eV and $E_g^{GaN} = 3.3$ eV [35].

Previous works done by Christensen [23] and Segev [24] show that a Gaussian shape at the all-electrons stage of the PP generation acts primarily on the lowest-energy 1s state, affecting then the higher-lying states and thus the energy gap through orthogonality of the wave functions. Based on this idea, we have decided to tune the local part (containing a Gaussian $\times$ polynomial function) of the relativistic separable dual-space Hartwigsen-Goedecker-Hutter (HGH) pseudopotentials [26] to correct the GaAs and GaN band gaps, as well as their X and L point eigenenergies. Our approach keeps then the non-local part of the PP unchanged, and avoid the regeneration through an all-electron stage of the PP. In particular, we adjust the r_{loc} and C_i coefficients in the local part of the pseudopotential,

$$V_{loc}(r) = \frac{-Z_{ion}}{r} erf\left(\frac{1}{\sqrt{2}}\bar{r}\right) + \exp\left(-\frac{1}{2}\bar{r}^2\right) \times$$
$$\times \left[C_1 + C_2\bar{r}^2 + C_3\bar{r}^4 + C_4\bar{r}^6\right], \quad (1)$$

where $\bar{r} = r/r_{loc}$, erf denotes the error function, and Z_{ion} is the ionic charge of the atomic core. The HGH nonlocal contributions, expressed in separable form, $V_l(r,r') = V_l(r)V_l'(r')$, where l is the angular momentum quantum number, were not changed from the initial *ab initio* scheme [26]. While the *ab initio* HGH pseudopotentials fix all the C_i coefficients to zero, we adjusted the Ga and As r_{loc} and C_i sets in order to fit (by least-squares minimization) the experimental GaAs electronic properties [35]: $E_-^=$1.52 eV, $\Delta L = E_L - E_- = 296$ meV, $\Delta X = E_X - E_- = 462$ meV and $m^* = 0.07m_e$ [4]. From Equation 1, one sees that the values of the polynomial coefficients will modify the potential seen by the s, p and d electrons, and so affect the band structure. The error on the experimental band structure parameters are so small (typically less than 10 meV from [35] and references within) they can be neglected in the chi-square method.

Convergence for the Kohn-Sham (KS) eigenvalues is achieved with a plane-wave cutoff energy of 25 Hartree. Keeping the cutoff energy at 25 Hartree [5], the r_{loc} and C_i coefficients of the N pseudopotential have been adjusted to fit the energy gap of the GaN crystal (keeping the Ga pseudopotential the same as that fitted in GaAs). We obtained an energy gap equal to its experimental value of 3.3 eV. The best relative positions of the X and L states have been found to be equal to $\Delta X = 1.1$ eV ($\Delta X^{exp} = 1.221$ eV) and

[3] The fcc 16 and 128-atom supercells correspond to a $2 \times 2 \times 2$ and $4 \times 4 \times 4$ fcc 2-atom primitive cells put together. The sc 64-atom supercell is built up with $2 \times 2 \times 2$ sc 8-atom supercells. The bcc 32-atom supercell is simply a $2 \times 2 \times 2$ bcc crystal. Throughout this article, a_0 is the conventional cubic lattice constant of the zincblende structure.

[4] Since the C_i coefficients are correlated, the approach do not suffer of a lack of observations (5 $\vec{k}$-points) compared to the number of free parameters (10 in GaAs and 5 in GaN). We indeed did not find $\chi^2 = 0$ with the number of free parameters used. Our final set of parameters was simply chosen as the global minimum of χ^2. Please note the original *ab-initio* HGH parameters give an energy gap of 0.492 eV for GaAs and of 2.317 eV for GaN, i.e. in close agreement with the values obtained from the TM pseudopotentials.

[5] For the N pseudopotential, full numerical convergence of the GaN Kohn-Sham eigenvalues required a cutoff of 75 Hartree. Nevertheless, our empirical approach allows us to consider the cutoff as a free parameter, fixed to a particular value which gives good convergence of the eigenvalues in the dilute nitride structures, where N concentration is very small ($x \in [0, 3.125]\%$).

	r_{loc}	C_1	C_2	C_3	C_4
Ga	0.4934	0.4404	0.2001	-0.0100	0.0099
As	0.6042	0.0321	0.6145	-0.1997	0.0007
N	0.2009	-6.4884	-5.3360	-2.5231	0.2675

Table 1: Values (in a.u.) of the adjusted coefficients, C_i and r_{loc}, in the local part of the empirical HGH pseudopotentials (Eq. 1) for Ga, As and N.

$\Delta L = 2.93$ eV ($\Delta L^{exp} = 2.29$ eV). Table 1 gives the values of r_{loc} and C_i obtained for the three atomic species considered. The corresponding local pseudopotentials are shown in Fig. 1. For the N atom, the significant difference between the empirical and original *ab initio* local part is needed to reproduce the experimental GaN energy gap, while keeping a good agreement with the experimental ΔX and ΔL predictions.

Figure 1: (color online) From the upper to the lower panel, the radial dependence of the local *ab initio* (dashed line) and empirical (solid line) HGH pseudopotentials $V_{loc}(r)$ for the Ga, As and N atoms, respectively.

Fig. 2 shows the band structure for GaAs, calculated with the Troullier-Martins *ab initio* pseudopotentials and with the empirically adjusted HGH pseudopotentials. Table 2 lists the important transition energies

Figure 2: (color online) Bulk GaAs band structure along the $L-\Gamma-X$ lines, calculated with the *ab initio* Troullier-Martins (dashed lines) and adjusted empirical HGH (solid lines) pseudopotentials. The top of the valence band (at the Γ point, $k=0$) has been chosen as the zero of energy.

and conduction band masses obtained. The relative positions ΔL and ΔX of the $L-$ and $X-$points from the conduction band edge (CBE) minimum (at $k = 0$) are in agreement with the experimental values (see Table 2). The energy gap matches the experimental value ($E_- = 1.42$ eV [35]) at $T = 300$ K. In addition, the deformation potential of the energy gap (measuring the change of the energy gap due to a hydrostatic deformation) is found to be equal to -8.58 eV, i.e. in good agreement with the experimental value, $a_g = -8.33$ eV [35]. (The same calculation with the *ab initio* TM pseudopotentials give a deformation potential equal to -8.02 eV.)

3. DFT optical Properties in ordered N configurations

Since we are concerned with the composition dependence of the optical properties in the dilute $GaAs_{1-x}N_x$ regime (nitrogen concentration $x \to 0$), we have studied the band dispersions around the $\Gamma-$point ($k = 0$) in large supercells (up to 512 atoms), where one As atom has been substituted by one N atom. Table 3 lists the eigenvalues at the $\Gamma-$point in a sc 64-atom supercell, for which the nitrogen concentration, $x = 3.125\%$. We see that the band-gap is substantially red-shifted from the pure GaAs value of 1.42 eV. Compared to the experimental redshifts, the rate of change, $(E_-(x) - E_-(x = 0))/x = 145$ meV/%, lies within the experimental range $\sim 100 - 200$ meV for $\sim 1\%$ of N added in GaAs [2, 3, 4, 1]. This large experimental range for dE_-/dx is explained by its large composition dependence (see next section for further details). In agreement with previous theoretical work of Wang *et al* [36] and Christensen *et al* [37], the 4-fold GaAs L conduction band edge (folding back to the $\Gamma-$point in a sc 64-atom supercell) splits into a singlet $a(L_{1c})$ and a triplet $t(L_{1c})$. The singlet lies 805 meV above the conduction band edge and 45 meV below the triplet. The 3-fold

	GaAs (LDA-TM)		GaAs (empirical-HGH)
E_-	0.515 eV (-66%)	E_-	1.424 eV (-6.3%)
ΔL	461 meV (56%)	ΔL	296 meV (0%)
ΔX	905 meV (96%)	ΔX	462 meV (0%)
m_e^*	0.034 m_e (-51%)	m_e^*	0.082 m_e (17.1%)

Table 2: Bulk GaAs LDA-DFT electronic properties obtained with the LDA Troullier-Martins (TM) norm-conserving pseudopotentials and our empirically adjusted HGH pseudopotentials. The values in brackets show the relative errors (in %), compared to the experimental data from [35].

states	a(Γ_{1c})	a(L_{1c})	t(L_{1c})	e(X_{1c})	a(X_{1c})
energy (eV)	0.973	1.778	1.823	1.835	1.984

Table 3: $GaAs_{1-x}N_x$ ($x = 3.125\%$) eigenvalues at the $\Gamma-$point ($\vec{k} = 0$) for the sc 64-atom supercell. The top of the valence band (at the Γ point, $k = 0$) has been chosen as the zero of energy.

GaAs X conduction band state also splits into a singlet $a(X_{1c})$ lying 149 meV above its doublet $e(X_{1c})$. The triplet state $t(L_{1c})$ is 12 meV below the doublet $e(X_{1c})$. In terms of the band anticrossing model (BAC) [16] (detailed further in this section), the presence of these singlet states induces an overall repulsion of the conduction band edge state $a(\Gamma_{1c})$, causing the large redshift of the energy gap observed.

In order to identify the DFT energy levels occurring in the optical transitions measured by photomodulated reflectance (PR) [14, 15] and electroreflectance (ER) [13], we compute the dipole transition matrix element squared, $I = | < \psi_i|\hat{p}|\psi_{VBM} > |^2$, between a selected conduction band i (i being $a(\Gamma_{1c})$, $a(L_{1c})$, $t(L_{1c})$, $e(X_{1c})$, etc.) and the valence band maximum (VBM). The magnitude of I identifies which conduction states participate in the optical transitions [38]. In the reciprocal space, the dipole matrix element at the $\Gamma-$point ($k = 0$) may be written as,

$$I(i, VBM) = \left| \sum_{\vec{G}} \vec{G} C_i^*(\vec{G}) C_{VBM}(\vec{G}) \right|^2 , \qquad (2)$$

where the sum runs over the vectors in the reciprocal lattice ($\vec{G}$), and where $C_i(\vec{G})$ and $C_{VBM}(\vec{G})$ are the coefficients of the plane-wave expansion of the conduction state i and top of the valence band state respectively. Figure 3 shows the dipole transition matrix elements between the different conduction states i and the VBM in the sc 64-atom supercell containing one N atom. All the dipole elements vanish, except for the state i corresponding to the singlet states $a(\Gamma_{1c})$, $a(L_{1c})$, $a(X_{1c})$. In particular, the $a(\Gamma_{1c}) \leftrightarrow VBM$ and $a(L_{1c}) \leftrightarrow VBM$ transitions are the largest, indicating that the transitions, $E_{\Gamma 1c} - E_{VBM}$ and $E_{L1c} - E_{VBM}$ are the good candidates for the experimentally observed E_- and E_+ transitions, respectively [14, 15, 13, 16].

Figure 3: DFT dipole transition matrix elements squared in arbitrary units from conduction state i to the top of the valence band (VBM) versus the energy $E_i - E_{VBM}$.

Table 4 gives the calculated composition dependence of the energy gap $E_-(x)$ and of $E_+(x) - E_-(x)$ for the empirical HGH (upper panel) and *ab initio* TM (lower panel) pseudopotentials. The following set of supercells have been used: sc 64-atom supercell at $x = 3.125\%$; fcc 128-atom supercell at $x = 1.5625\%$; sc 216-atom supercell at $x = 0.9259\%$; bcc 256-atom supercell at $x = 0.78125\%$; sc 512-atom supercell at

Empirical pseudopotential

x	3.125	1.5625	0.9259	0.78125	0.3906	0.0
E_-	0.973 (45)	1.033 (40)	1.262 (66)	1.293 (69)	1.348 (77)	1.4257 (100)
$(E_-(x) - E_-(0))/x$	14.5	25.1	17.7	17.0	19.9	—
$E_+ - E_-$	806 (41)	634 (50)	477 (30)	369 (23)	300 (17)	—

ab initio pseudopotentials

x	3.125	1.5625	0.9259	0.78125	0.3906	0.0
$E_- = E_-^{GaAsN}$	0.146 (56)	0.221 (54)	0.406 (81)	0.426 (84)	0.472 (91)	0.515 (100)
$(E_-(x) - E_-(0))/x$	11.8	18.8	11.8	11.4	11.1	—
$E_+ - E_-$	823 (35)	633 (38)	580 (16)	475 (11)	437 (5)	—

Table 4: Values of $E_-(x)$, $(E_-(x) - E_-(0))/x$ (in eV), and $E_+(x) - E_-(x)$ (in meV), for the optical transitions, $E_-(x)$ and $E_+(x)$, in $GaAs_{1-x}N_x$, as functions of nitrogen concentration x (in %), calculated in DFT with empirical HGH pseudopotentials (upper panel) and *ab initio* TM pseudopotentials (lower panel). The values in brackets indicate the $\Gamma-$character (in %) of the states, $a(\Gamma_{1c})$ (2nd row) and $a(L_{1c})$ (4th row), at each concentration.

$x = 0.3906\%$ and 2-atom fcc primitive cell at $x = 0\%$. For the states $a(\Gamma_{1c})$ and $a(L_{1c})$, we have calculated the GaAs Γ-character as the overlap, $|\langle\psi|\Gamma_{1c}\rangle|^2$, with the pure GaAs conduction band edge Γ_{1c} state.

Concerning the energy gap variation, $(E_-(x) - E_-(0))/x$, both *ab initio* and empirical pseudopotentials provide theoretical predictions in reasonable agreement with the experimental range $\sim 100 - 200$ meV for $\sim 1\%$ of N added in GaAs [2, 3, 4, 1]. Only the value from the fcc 128-atom supercell deviates substantially from the mean values of 173 meV/% (empirical pseudopotential) and 117 meV/% (*ab initio* pseudopotential). This deviation is explained by the large repulsive N-N strain interaction along the [110]−direction dominating in this fcc structure [22].

Figure 4 shows the calculated composition-dependence of the optical transition energies, $E_-(x)$ and $E_+(x)$. Based on earlier work of Shan *et al* [16], O'Reilly *et al* [39] reported that the composition dependence of the E_- and E_+ energy levels may be described by the band anti-crossing (BAC) Hamiltonian,

$$\hat{H}_{BAC} = \begin{vmatrix} E_N + (\alpha - \Delta)x & \beta\sqrt{x} \\ \beta\sqrt{x} & E_c + (\alpha + \Delta)x \end{vmatrix}, \tag{3}$$

where the matrix element [40], $V = \beta\sqrt{x}$, describes the interaction between a resonant localized N impurity level E_N and the bulk GaAs conduction band edge E_c. The eigenvalues of $\hat{H}_{BAC}$,

$$E_\pm = \frac{(E_c + E_N)}{2} + \alpha x \pm \sqrt{\left(\frac{E_c - E_N}{2}\right)^2 + [\beta^2 - \Delta(E_N - E_c)]\,x + \Delta^2 x^2}, \tag{4}$$

correspond then to the E_- and E_+ optical transition energies. Fixing the value of E_c at the DFT energy gap of GaAs, $E_-(x = 0)$, the calculated DFT E_+ and E_- values have been fitted with Eq. (4) by the least-squares method, using E_N, α, β and Δ as free parameters. The results of the fit are shown in Figure 4 for the empirical HGH pseudopotential (upper graph) and the *ab initio* pseudopotential (lower graph). For the empirical pseudopotentials, $E_N - E_c = 158$ meV, $\beta = 2.25$ eV, $\alpha = -4.9$ eV and $\Delta = 11$ meV. Corresponding experimental values are $E_N - E_c = 150 - 180$ meV from Ref. [41] or $E_N - E_c = 220 - 230$ meV and $\beta = 2.6 - 2.7$ eV from Refs. [43, 45, 46]. We see that the empirical pseudopotential BAC parameters are in agreement with the experimental predictions from Wolford *et al.* [41] for the position of E_N. The interaction parameters β is slightly underestimated, due to the linear contribution α added in the O'Reilly approach [6]. For the *ab initio* pseudopotentials, $E_N - E_c = 367$ meV, $\beta = 2.07$ eV, $\alpha = -5.25$ eV and

[6] Fitting E_- with the parametric dependence used by Walukiewicz [43], we obtained $E_N - E_c = 600$ meV and $\beta = 4.1$ eV.

$\Delta = -18$ meV (E_c being equal to 0.515 eV here). The large $E_N - E_c$ value is due to the overestimation of $E_{L_{1c}} - E_{\Gamma_{1c}}$ by the *ab initio* TM pseudopotentials (see Table 2). On the other hand, the other BAC parameters (β, α and Δ) are close to the values derived with the empirical pseudopotentials.

Figure 4: (color online) Calculated nitrogen composition dependence of E_+ and E_- transitions, fitted with the BAC model. The dashed and solid lines show the fitted $E_+(x)$ and $E_-(x)$, respectively, from Eq.4, with the parameters given in the text. The calculated energies (circles and stars) have been computed with the empirical HGH (upper graph) and *ab initio* TM (lower graph) pseudopotentials.

4. DFT optical Properties in disordered N configurations

To determine the effect of a random distribution of N atoms in the dilute nitrides on the optical properties, we have studied bcc 256-atom supercells, where 2, 3 and 4 As atoms have been randomly substituted by N atoms, covering thus the nitrogen concentrations $x = 1.5625\%$, $x = 2.34375\%$ and $x = 3.125\%$ respectively. The relaxed atomic positions have been computed with the VFF approach (see Appendix). Lattice constants have been assumed to follow the Vegard's law [8]. Using our empirical pseudopotentials, the DFT band structures have been calculated on a set of 15 randomly generated N atomic configurations for each concentration ($x = 1.5625\%$, $x = 2.34375\%$ and $x = 3.125\%$).

At a given concentration, we have calculated the dipole transition matrix elements (Equation 2) for the 15 individual N configurations: $I_\nu(E_i, E_{VBM})$ where $\nu = 1, \cdots, 15$ and i (VBM) denotes the conduction band (valence band maximum) index with energy E_i (E_{VBM}). The histograms in Figure 5 have then been obtained by binning the contributions from the 15 random configurations,

$$I_{tot}(E, E_{VBM}) = \sum_{\nu=1}^{15} I_\nu(E_i, E_{VBM})$$

on the energy axis E. The bin width is 50 meV. On each individual histogram (at $x = 1.5625\%$, $x = 2.34375\%$ and $x = 3.125\%$), two prominent peaks, associated with the E_- and E_+ levels, can be observed. We fit each of these peaks with a Gaussian (mean μ and standard deviation σ) to obtain the peak positions and widths indicated in Fig. 5 [7].

Compared to the optical transitions computed in the ordered supercells (Table 4), we find the random distributions of N significantly increase the energy gap (by 186 meV at $x = 1.5625\%$ and 121 meV at $x = 3.125\%$) while the E_+ transitions are only slightly affected (+28 and +15 meV at $x = 1.5625\%$ and $x = 3.125\%$, respectively) by the nature of the N configuration. Figure 6 shows the composition dependence

Figure 5: (color online) Calculated histogram of the total dipole transition matrix elements $I_{tot}(E, E_{VBM})$ (in arbitrary units) from conduction states at energy E to the top of the valence band (VBM) for random configurations of N in a 256-atom supercell, at N concentrations of $x = 1.5625\%$ (top panel), $x = 2.34375\%$ (middle panel) and $x = 3.125\%$ (bottom panel). The value of μ and σ beside each prominent peak of the histogram indicate the central energy and width, respectively, of the peak.

of the E_- and E_+ energy levels calculated from these N randomly distributed supercells, together with the levels computed in the dilute limit at $x = 0.78125\%$ (1 N in a bcc 256-atom supercell) and $x = 0.390625\%$ (1 N in a sc 512-atom supercell). The best fit of the BAC model energies to these calculated values of $E_-(x)$ (solid line) and $E_+(x)$ (dashed line) has

$$E_N - E_c = 147 \text{ meV}, \beta = 1.88 \text{ eV}, \alpha = -2.0 \text{ eVand } \Delta = 0 \text{ meV}. \quad (5)$$

[7] We found a maximal variation of 25 meV for E_+ and E_- (μ) when the bin width varies from 10 to 80 meV, or when the number of samples varies from 10 to 15.

If one includes the errors on the free parameters got from the chi-square method (errors estimated by increasing by one unit the normalized χ^2 value around its minimal value [44]), we find that all the parameters derived with the three approaches are identical within the estimated error bars (*ab-initio* pseudopotentials: $E_N - E_c = 367 \pm 75$ meV, $\beta = 2.07 \pm 0.5$ eV, $\alpha = -5.25 \pm 2.7$ eV; empirical pseudopotentials + ordered configurations: $E_N - E_c = 158 \pm 85$ meV, $\beta = 2.25 \pm 0.41$ eV, $\alpha = -4.9 \pm 2.75$ eV; empirical pseudopotentials + disordered configurations: $E_N - E_c = 147 \pm 22$ meV, $\beta = 1.88 \pm 0.10$ eV, $\alpha = -2.00 \pm 0.61$ eV). Only the position of the localized nitrogen level $E_N - E_c$ computed with the LDA pseudo potentials is in disagreement with the other two theoretical (empirical pseudopotentials + ordered or disordered N configuration) and the experimental predictions $E_N - E_c = 150 - 180$ meV from Ref. [41] or $E_N - E_c = 220 - 230$ meV from Refs. [43, 45, 46]. Therefore, the LDA approach must be rejected for any predictions of the composition dependence of E_- and E_+.

Comparing the ordered and disordered approaches, the empirical PP combined with the disordered structures gives a better estimation (reduces the errors) of the BAC parameters. In addition, these parameters are in better agreement with the derived parameters obtained by Lindsay *et al.* from tight-binding (TB) calculations ($\beta^{TB} = 1.95$ eV, $\alpha^{TB} = -1.3$ eV and $\Delta^{TB} = 0$ meV) [47]. Therefore, the BAC parameters obtained from the empirical pseudopotentials + disordered approach can be chosen to define (through Eq. 4 and parameters listed in Eq. 5) a DFT-based analytical expression of the composition dependence of the $E_+(x)$ and $E_-(x)$ states.

Concerning the experimental discrepancy between Ref. [41] and Refs. [43, 45, 46], since no experimental errors are provided, we can only conclude that our calculations agree with the results obtained by Wolford et al [41].

Figure 6: (color online) Average E_+ and E_- energies, computed for random N atomic configurations at N concentrations, $x = 1.5625\%$, $x = 2.34375\%$ and $x = 3.125\%$. The values in the dilute limit, $x = 0.78125\%$ and $x = 0.390625\%$, are also included (see text). The dashed and solid lines show the best fit of $E_+(x)$ and $E_-(x)$, respectively, within the BAC model (Eq.4).

Complementing our analysis of the composition dependence of the energy gap E_-, and motivated by its theoretical importance in determining the transport properties (see introduction), Figure 7 shows the composition dependence of the energy gap, its first derivative dE_-/dx obtained from fitted energy dependence (Eq. 4) for the three previous schemes: (1) *ab initio* pseudopotential and (2) empirical pseudopotential applied to the supercells containing N ordered configuration, and (3) empirical pseudopotential applied to the supercells with the N atoms randomly distributed. On the same figure, two direct fits (from [43] and [42] and references within for the experimental data) on the experimental energy gaps are also given. In particular, the thin solid line on Figure 7 has been taken from Walukiewicz [43] and the thin dashed line from Tisch *et al.* [42]. To provide an estimation of the variance of the experimental energy gaps, we found that all the experimental energy gaps given in [43] follow its fitting curve (thin solid line) within 40 meV (indicated on Figure 7 by the grey surface). Since we did not find in the literature any experimental estimation of the error on dE_-/dx, such informations are then omitted in our analysis.

On Figure 7-upper graph, one clearly sees that the *ab initio* pseudopotentials (thick dashed line) gives a good agreement with the experimental results for the composition dependence of the energy gap (shifted by its values at $x = 0$). Nevertheless, its first derivative dE_-/dx (Figure 7-lower graph) shows the *ab initio* pseudopotentials (dashed curve) fail to reproduce the experimental dE_-/dx (thin solid and dashed curves) dependence in both the dilute ($x \leq 1\%$) and alloy ($x \geq 1\%$) regimes. On the other hand, the empirical pseudopotential applied to the ordered structures (solid line on Figure 7-lower graph) improves the slope of the energy gap variation in the dilute limit. The discrepancy in the alloy regime is removed for both the composition dependence of the energy gap (thick dotted line on Figure 7-upper graph) and its first derivative (thick dotted line on Figure 7-lower graph) only if one applies the empirical pseudopotential to

the supercells containing a random distribution of N atoms on group $V-$sites. Therefore, any physical properties depending on dE_-/dx such as the scattering cross section [18] need to be studied using both the empirical pseudopotential and a random N distribution.

Figure 8 compares the composition dependence of the DFT $E_+ - E_-$ energy separations computed

Figure 7: (color online) From the top to the bottom: Composition dependence of the energy gap and the first derivative dE_-/dx calculated with the *ab initio* pseudopotential (dashed line) and the empirical pseudopotential (solid line) in ordered supercells, and the empirical pseudopotential in disordered supercells (dotted line). The fit to the experimental data have been taken from Tisch *et al.* [42] (thin dashed line + grey zone, see text) and Walukiewicz *et al* (thin solid line) [43].

with the three previous schemes to the experimental data [14, 13, 15, 16], as well as to previous theoretical works using "artificial Darwin shifts" [37], a strain-dependent functional form of the pseudopotential [48] or standard ab initio Bachelet pseudopotentials [49]. In particular, Szwacki and Boguslawski [49] obtained the same agreement to the experimental data than our ab initio approach (dashed line on Fig. 8). Regarding to the works done by Christensen *et al.* [37], we also obtain the same results with our empirical approach in the ordered structures (solid line on Fig. 8). Nevertheless, our comparison between both LDA and EPM schemes (dashed and solid lines on Fig. 8) shows that a deviation from the empirical predictions appears in the dilute limit ($x \leq 1\%$), where the *ab initio* pseudopotentails fail to reproduce the experimental position of the L state relative to the energy gap in pure GaAs. Beyond the LDA and EPM schemes in the N ordered configurations, our random approach (dotted line on Fig. 8) shows that the large $(E_+ - E_-)(x)$ local variations due to the different N symmetry configurations are now removed. Nevertheless, our theoretical $E_+ - E_-$ energy separations (EPM+N disordered) then agree less (but still within 20%) with the experimental data. We therefore point out that the random N configurations (modeling better the experimental crystal than the ordered supercells) underestimate the experimental energy separations. Mattila *et al.* [48] also studied in the dilute limit ($x < 0.8\%$) these optical properties with randomly distributed N configurations. They obtained a better agreement then us to the experimental data, which is explained by their definition of the E_+ as a weighted average of the two a(N) and a(L_{1c}) levels based on their Gamma character [48]. Nevertheless, according to Christensen *et al.*, Szwacki and Boguslawski [49] and the experimental evidences from Cheong *et al.* [50], the L-related character of E_+ suggests to associate E_+ to the a(L_{1c}) level only. By defining E_+ as the first well-defined peak beyond E_- in the dipole transition matrix elements I (see Fig. 5), we actually recover this property (see Fig. 3) in the N ordered limit (Christensen [37] and Szwacki [49] cases).

Figure 8: (color online) Energy separation between the E_+ and E_- levels versus the nitrogen atomic concentration, computed with the *ab initio* pseudopotential (dashed line), the empirical pseudopotential (solid line) and the empirical pseudopotential in disordered supercells (dotted line); Circles correspond the experimental data taken from [13]; Triangles to the experimental data taken from [14] and [16] respectively; Diamonds to the experimental data taken from [15].

5. Conclusions

Using first-principles total energy calculations, optical properties have been computed for various concentrations x of N in GaN_xAs_{1-x} supercells. By modifying the local part of the Hartwigsen-Goedecker-Hutter (HGH) pseudopotentials, an empirical scheme has been defined to remove the LDA underestimation of the energy gap and reproduce the correct energies of the L and X states in GaAs.

Three schemes for finding the optical transitions have been considered and compared: (1) *ab initio* pseudopotentials (PP) and (2) empirical PP applied to supercells containing an ordered configuration of N atoms, and (3) empirical PP applied to supercells with a random distribution of N atoms. In agreement with previous theoretical approaches [49, 37, 48], the calculations of the dipole transition matrix elements allow

us to identify the singlet $a(\Gamma_{1c})$ and $a(L_{1c})$ states with the experimental optical E_- and E_+ transitions, measured by electroreflectance (ER) or photomodulated reflectance (PR) [13, 14, 15]. We find agreement with the experimental composition dependence of the $E_+ - E_-$ energy separation for the DFT calculations, computed with the three different schemes.

Concerning the composition dependence of the energy gap and its first derivative with respect to x, we conclude that only the third scheme involving the empirical pseudopotentials combined with a random distribution of N atoms, can be used to match the experimental composition dependence of the energy gap E_- and its first derivative dE_-/dx. Therefore, any physical properties depending on dE_-/dx such as the carrier scattering cross section [18], must be studied by considering both the empirical corrections to the *ab initio* pseudopotentials (or some other correction of the DFT band structure) and supercells containing a random distribution of N atoms. This is consistent with the conclusions of previous authors [22, 51, 21] concerning the interaction between nitrogen atoms in this alloy. Please note our empirical HGH pseudopotentials were constructed to reproduce with a good accuracy the optical and electronic properties of GaAsN in the dilute limit. Nevertheless, further investigations need to be done in order to asses the transferability of our empirical HGH pseudopotentials in a larger composition range.

By comparing our DFT results with the band anticrossing (BAC) model, we also provide DFT-based analytical expressions for the composition dependence of the energy gap and the E_+ states, which agree with experiments within 20% for $(E_+ - E_-)(x)$.

6. acknowledgments

The authors wish to acknowledge the SFI/HEA Irish Centre for High-End Computing (ICHEC) for the provision of computational facilities and support. This work has been supported by Science Foundation Ireland.

A. Determination of the free parameters of the VFF model

In order to avoid very time-consuming structural optimization, we have used the valence force field (VFF) method (with parameters fitted to smaller DFT-optimized structures) to find the relaxed atomic positions in very large supercells. Within the VFF model implemented in the `GULP` [52] program, two- and three-body harmonic potentials are used to model the interatomic interactions, including nearest-neighbor interactions only. In particular, the potentials may be written as,

$$V_{2-body}(r) = \frac{1}{2}k_r(r - r_0)^2, \tag{6}$$

where r is the distance between neighboring atoms, and

$$V_{3-body} = \frac{1}{2}k_\theta(\theta - \theta_0)^2, \tag{7}$$

where θ is the angle between a pair of tetrahedral bonds on a given atom. The parameters k_r and k_θ specify bond-stretching and bond-bending forces, respectively, for a given bond type. The parameters r_0 and θ_0 are equal to the equilibrium values of r and θ in the simplest, physically motivated model, although they can be treated as arbitrary fitting parameters, without imposing this physical interpretation. For the various types of bonds, k_r^{AB} is the bond stretching parameter for bonds between type A and type B atoms, and k_θ^{ABC} is the bond bending parameter between an A-B and a B-C bond, centered on a B-type atom. The set of free parameters,

$$\begin{aligned} &k_r^{GaAs}, r_0^{GaAs}, k_r^{GaN}, r_0^{GaN}, k_\theta^{AsGaAs}, \theta_0^{AsGaAs}, \\ &k_\theta^{NGaN}, \theta_0^{NGaN}, k_\theta^{NGaAs}, \theta_0^{NGaAs}, \end{aligned} \tag{8}$$

have been adjusted by

2-body	Ga-As	Ga-N	
k_r (eV/Å^2)	7.99	18.5	
r_0 (Å)	2.4454635	1.9414878	
3-body	As-Ga-As	N-Ga-N	As-Ga-N
k_θ (eV/rad^2)	3.1304	3.248	3.192
θ_0 (°)	109.471	109.471	109.471

Table 5: Values of the free parameters (used in `GULP`) which fit the Ga-As and Ga-N bond lengths computed from first principles calculations in a cubic 64-atom supercell.

Ga-N (Å)	$x = 0.25$	$x = 0.125$	$x = 0.0625$	$x = 0.03125$	$x = 0.015625$
VFF (Ref. [30])	2.0172 (1.72)	2.0563 (2.05)	2.0205 (0.70)	2.0273 (1.01)	2.0309 (1.16)
VFF (Table 5)	2.0381 (0.70)	2.0761 (1.10)	2.0397 (0.24)	2.0481 (0.01)	2.0517 (0.15)
DFT (`Abinit`)	2.0525	2.09925	2.0347	2.0480	2.0548
E_- (eV)	$x = 0.25$	$x = 0.125$	$x = 0.0625$	$x = 0.03125$	$x = 0.015625$
VFF (Ref. [30])	-	-	0.198 (11.6)	0.203 (14.3)	0.263 (14.0)
VFF (Table 5)	-	-	0.238 (6.2)	0.240 (1.3)	0.2995 (2.1)
DFT (`Abinit`)	-	-	0.224	0.237	0.306

Table 6: Composition dependence of the Ga-N bond lengths and energy gaps. The values in brackets give the relative error (in percent) from the LDA-DFT results.

1. fixing the values of the VFF coefficients to those proposed by Martin [30],
2. adjusting the values of r_0 in Eq. 6 such that it reproduces the GaAs and GaN lattice constant obtained with `Abinit`,
3. keeping the values of θ_0 in Eq. 7 equal to the tetrahedral angle $\theta_0 = 109.47°$,
4. imposing the Vegard's law during the VFF relaxation, and so avoiding a bowing in the lattice constant as a function of the nitrogen concentration,
5. adjusting the k_θ coefficients to reproduce the DFT Ga-As and Ga-N bond lengths computed in a 64-atom supercell. These coefficients have been multiplied by an identical factor ($k'_\theta = \alpha k_\theta$), so preserving the same ratio as the Martin's original coefficients in Ref. [30]. This guarantees that the structure formed by the N and its four nearest Ga atoms corresponds to a perfect tetrahedron.

Table 5 lists the values of the adjusted VFF parameters. Table 6 shows the good agreement through the values of the GaN bond lengths and energy gaps between different structures relaxed with VFF (with the Martin coefficients or the new set of parameters) and LDA-DFT.

References

[1] W. G. Bi and C. W. Tu, Appl. Phys. Lett. **70** (1997) 1608.
[2] M. Weyers, M. Sato and H. Ando, Jpn. J. Appl. Phys., Part 1 **31** (1992) 853.
[3] M. Weyers and M. Sato, Appl. Phys. Lett. **62** (1993) 1396.
[4] M. Kondow, K. Uomi, K. Hosomi and T. Mozume, Jpn. J. Appl. Phys. **33** (1994) L1056.
[5] L. Bellaiche, S.-H. Wei and A. Zunger, Phys. Rev. B **54** (1996) 17568.
[6] I. Suemune, K. Uesugi and T.-Y. Seong, Semicond. Sci. Technol. **17** (2002) 755.
[7] M. Reason, X. Weng, W. Ye, D. Dettling, S. Hanson, G. Obeidi and R. S. Goldman, J. Appl. Phys. **97** (2005) 103523.
[8] G. Stenuit and S. Fahy, Phys. Rev. B **76** (2007) 035201.
[9] P. N. Hai, W. M. Chen, I. A. Buyanova, H. P. Xin and C. W. Tu, Appl. Phys. Lett. **77** (2000) 1843.
[10] A. Lindsay and E. P. O'Reilly, Phys. Rev. Lett. **93** (2004) 196402.
[11] A.M. Teweldeberhan and S. Fahy, Phys. Rev. B **72** (2005) 195203.
[12] A.M. Teweldeberhan and S. Fahy, Phys. Rev. B **73** (2006) 245215.
[13] J.D. Perkins, A. Mascarenhas, Y. Zhang, J.F. Geisz, D.J. Friedman, J.M. Olson and S.R. Kurtz, Phys. Rev. Lett. **82** (1999) 3312.

[14] W. Shan, W. Walukiewicz, K.M. Yu, J.W. Ager III, E.E. Haller, J.F. Geisz, D.J. Friedman, J.M. Olson, S.R. Kurtz and C. Nauka, Phys. Rev. Rev. **62** (2000) 4211.
[15] P.J. Klar, H. Grunïng, W. Heimbrodt, J. Koch, F. Höhnsdorf, W. Stolz, P.M.A. Vicente and J. Camassel, Appl. Phys. Lett. **76** (2000) 3439.
[16] W. Shan, W. Walukiewicz, J.W.Ager III, E.E. Haller, J.F. Geisz, D.J. Friedman, J.M. Olson and S.R. Kurtz, Phys. Rev. Lett. **82** (1999) 1221.
[17] F. Mandl, *Quantum Mechanics* (Butterworths, London, 1957), p. 142ff.
[18] S. Fahy and E.P. O'Reilly, Appl. Phys. Lett. **83** (2003) 3731.
[19] F. Murphy-Armando and S. Fahy, Phys. Rev. Lett. **97** (2006) 096606.
[20] S. Joyce, F. Murphy-Armando, and S. Fahy, Phys. Rev. B **75** (2007) 155201.
[21] S. Fahy, A. Lindsay, H. Ouerdane, and E.P. O'Reilly, Phys. Rev. B **74** (2006) 035203.
[22] P.R.C. Kent and A. Zunger, Phys. Rev. B **64** (2001) 115208.
[23] N.E. Christensen, Phys. Rev. B **30** (1984) 5753.
[24] D. Segev, A. Janotti and C.G. Van de Walle, Phys. Rev. B **75** (2007) 035201.
[25] N. Troullier and J.L. Martins, Phys. Rev. B **43** (1991) 1993.
[26] C. Hartwigsen, S. Goedecker and J. Hutter, Phys. Rev. B **58** (1998) 3641.
[27] P. Hohenberg and W. Kohn, Phys. Rev. **136** (1964) B864.
[28] W. Kohn and L. J. Sham, Phys. Rev. **140** (1965) A1133.
[29] M. C. Payne, M. P. Teter, D. C. Allan, T. A. Arias and J. D. Joannopoulos, Rev. Mod. Phys. **64** (1992) 1045.
[30] R. M. Martin, Phys. Rev. B **1** (1970) 4005.
[31] X. Gonze, J.-M. Beuken, R. Caracas, F. Detraux, M. Fuchs, G.-M. Rignanese, L. Sindic, M. Verstraete, G. Zerah, F. Jollet, M. Torrent, A. Roy, M. Mikami, Ph. Ghosez, J.-Y. Raty, D.C. Allan, Computational Materials Science **25** (2002) 478-492; The ABINIT code is a common project of the Université Catholique de Louvain, Corning Incorporated, the Université of Liège, and other contributors (`URL http://www.abinit.org`).
[32] W. G. Aulbur, L. Jönsson and J. W. Wilkins, Materials Science: Review of Quasiparticle Calculations: Overview `URL http://www.physics.ohio-state.edu/ ∼aulbur/gw/review0.html`.
[33] M.S. Hybertsen and S. Louie, Phys. Rev. B **34** (1986) 5390.
[34] F. Aryasetiawan and O. Gunnarson, Rep. Prog. Phys. **61** (1998) 237-312.
[35] I. Vurgaftman, J. R. Meyer and L. R. Ram-Mohan, Appl. Phys. Rev. **89** (2001) 5815.
[36] L.-W. Wang, Appl. Phys. Lett. **78** (2001) 1565.
[37] N.E. Christensen, I. Gorczyca and A. Svane, J. Phys. Chem. Solids **67** (2006) 1948.
[38] L. Bellaiche, S.-H. Wei, and A. Zunger, Phys. Rev. B **56** (1997) 10233.
[39] E.P. O'Reilly, A. Lindsay, S. Tomić and M. Kamal-Saadi, Semicond. Sci. Technol. **17** (2002) 870.
[40] A. Lindsay and E.P. O'Reilly, Solid State Commun. **112** (1999) 443.
[41] D.J. Wolford, J.A. Bradley, K. Fry and J. Thompson, in *Proceedings of the 17th International Conference of the Physics of Semiconductors*, edited by J.D. Chadi and W.A. Harrison (Springer, New York, 1984), p. 627.
[42] U. Tisch, E. Finkman and J. Salzman, Appl. Phys. Lett. **81** (2002) 463.
[43] W. Walukiewicz, Physica E **20** (2004) 300-307.
[44] R. Barlow, 2004 Asymmetris errors *Preprint* physics/0401042.
[45] C. Skierbiszewski, Semicond. Sci. Technol. **17** (2002) 803-814.
[46] A. Grau, T. Passow and M. Hetterich, Appl. Phys. Lett. **89** (2006) 202105.
[47] A. Lindsay and E.P. O'Reilly, Solid State Commun. **118** (2001) 313-317.
[48] T. Mattila, S-H Wei and A. Zunger, Phys. Rev. B **60** (1999) R11245.
[49] N. Gonzalez Szwacki and P. Boguslawski, Phys. Rev. B **64** (2001) 161201(R).
[50] H.M. Cheong, Y. Zhang, A. Mascarenhas and J.F. Geisz, Phys. Rev. B **61** (2000) 13 687.
[51] L. Bellaiche, S.-H. Wei, and A. Zunger, Appl. Phys. Lett. **70** (1997) 3558 .
[52] J. D. Gale, J. Chem. Soc., Faraday Trans., **93**(4) (1997) 629-637.